Intraseasonal Variability in the NASA GISS General Circulation Model

Daehyun Kim[1], Adam H. Sobel[1,2], Yonghua Chen[3,4], and Anthony Del Genio[4]

[1]Lamont-Doherty Earth Observatory of Columbia University, New York, NY
[2]Department of Applied Physics and Applied Mathematics, Columbia University, New York, NY
[3]Department of Earth and Environmental Sciences, Columbia University, New York, NY
[4]NASA Goddard Institute for Space Studies, New York, NY

Abstract

The tropical precipitation simulated by different versions of the atmospheric model of the Goddard Institute for Space Studies (GISS) general circulation model (GCM) – Model_E is examined in this study. The mean state, intraseasonal variability, and wavenumber-frequency power spectra are calculated and compared to observations. The new AR5 model shows clear improvement compared to AR4 in magnitude of intraseasonal variability. Although there is significant improvement in the magnitude of intraseasonal variability of and simulation of the Kelvin mode, it is shown that AR5 still lacks the MJO mode, which dominates intraseasonal variability and interacts with many other climate components (e.g. tropical cyclone, Asian/Australian summer monsoon) in nature. As consistent with previous studies, simulation fidelity of the MJO strongly depends on cumulus parameterization. With enhanced overall entrainment rate in the convection scheme, Model_E simulates precipitation variability related with the MJO space-time scale. MJO life-cycle composite and process oriented diagnostics show that the interaction between moisture and convection is strengthened when entrainment rate is enhanced.

Experimental design

EXP	Description
AR4	AGCM component of the AR4 version
AR5	AGCM component of the AR5 version
A22	Same as AR5, except for higher entrainment rate, without fraction constrain, one plume per each cloud base

$$\varepsilon = \frac{C_\varepsilon a B}{w_c^2}$$

entrainment rate (ε); constants ($C_\varepsilon a$); buoyancy (B); vertical velocity (w_c)

Gregory (2001)

Mean and intraseasonal variability

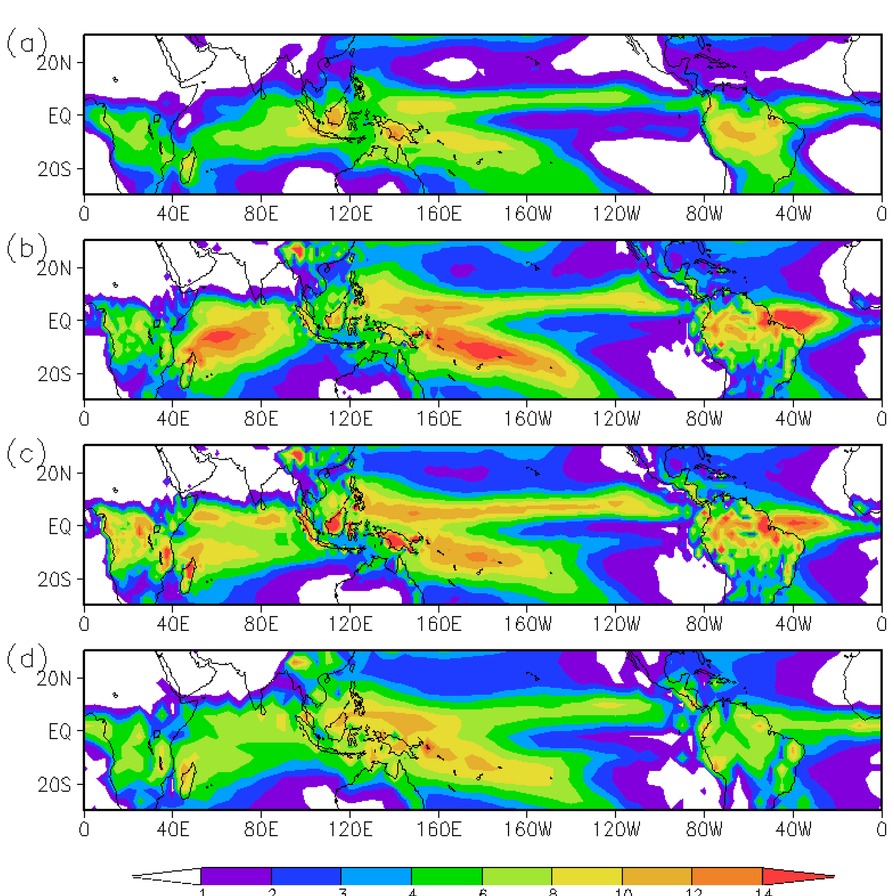

FIG. 1. November–April mean precipitation (mm day^{-1}) of (a) GPCP, (b) A22, (c) AR5, and (d) AR4

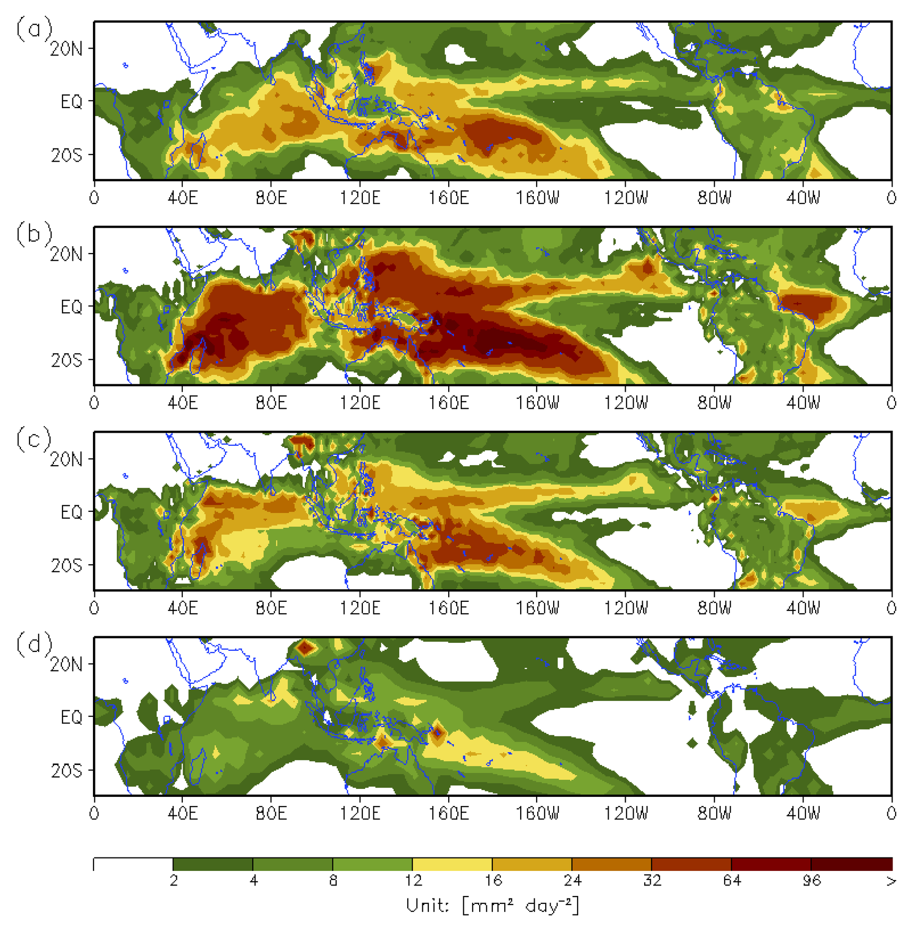

FIG. 2. Variance of 20–100-day bandpass filtered precipitation(mm^2 day^{-2}) of (a) GPCP, (b) A22, (c) AR5, and (d) AR4

Wavenumber-frequency diagram

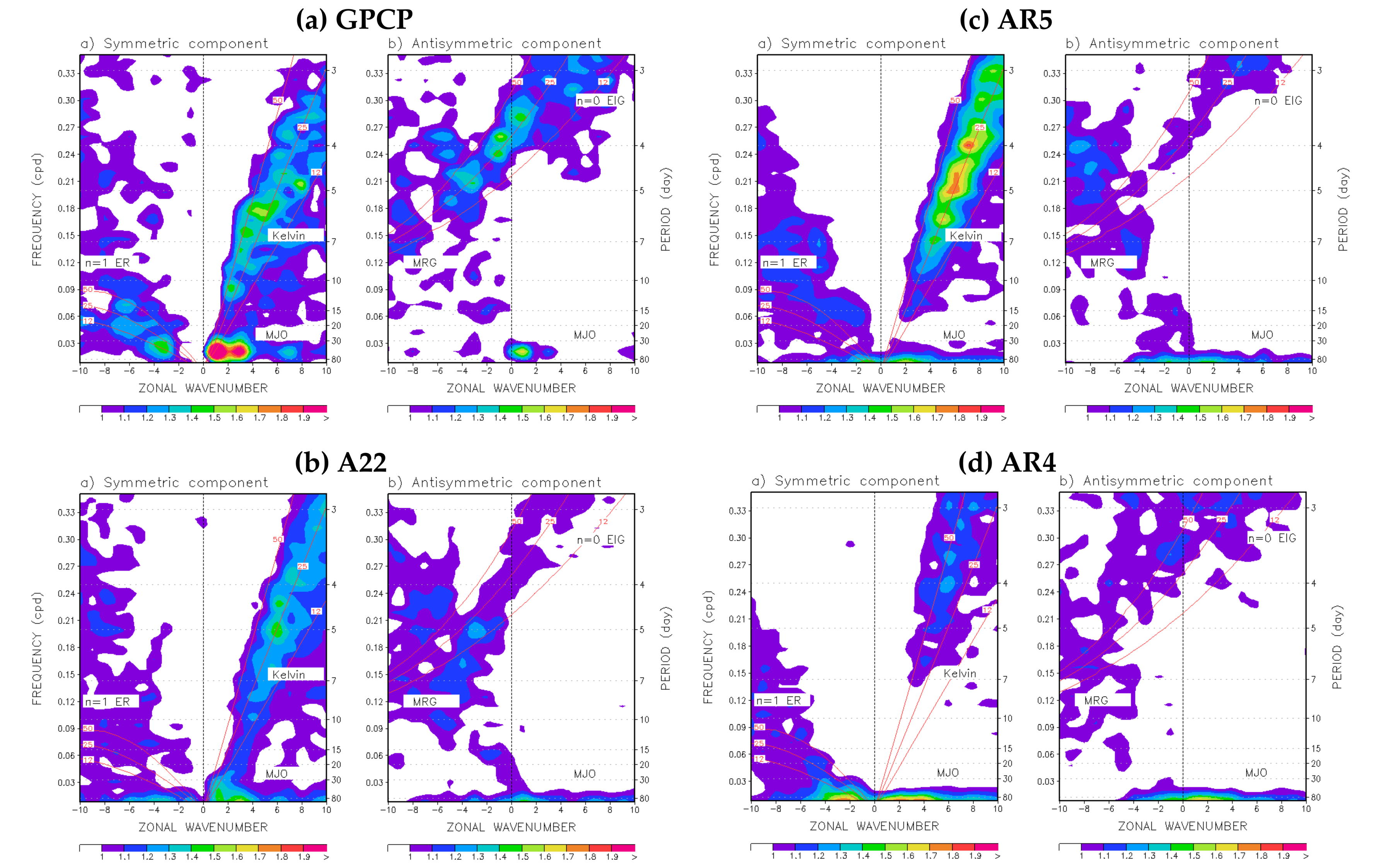

FIG. 3. Space–time spectrum of the 15°N–15°S symmetric and antisymmetric component of precipitation divided by the background spectrum. (a) GPCP, (b) A22, (c) AR5, and (d) AR4. Superimposed are the dispersion curves of the odd meridional mode numbered equatorial waves for the five equivalent depths of 12, 25, and 50m

MJO life-cycle composite

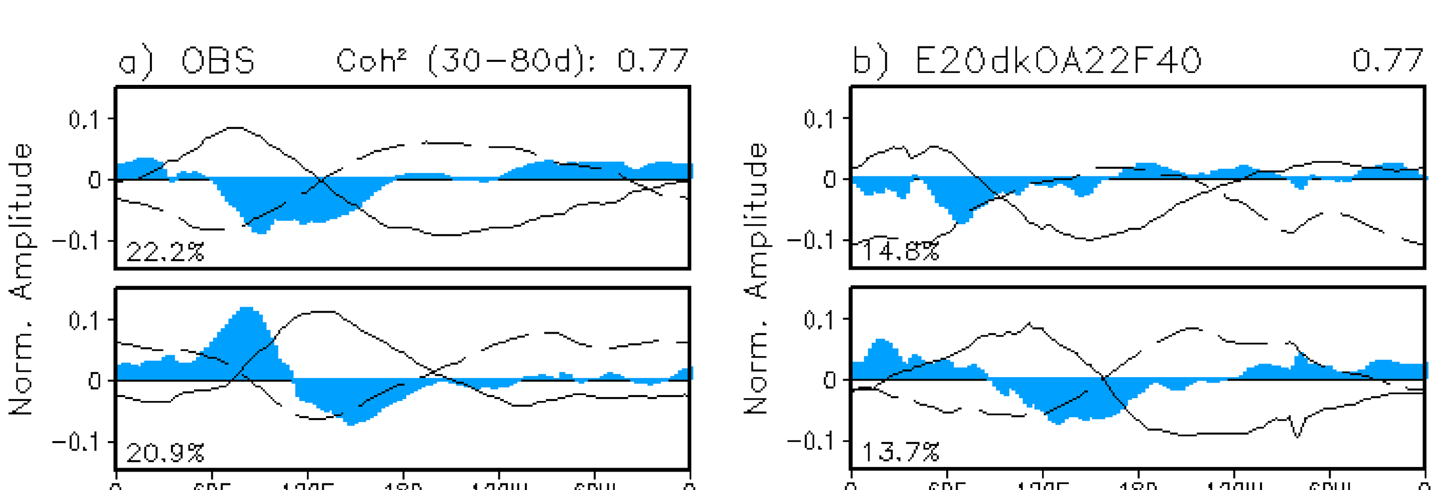

FIG. 4. First two CEOF modes of 20–100-day 15ºS–15ºN averaged 850-hPa and 200-hPa zonal wind and OLR for the (a) NCEP/NCAR and AVHRR, (b) A22. The total variance explained by each mode is shown in the lower left of each panel. The mean coherence squared between principal components of two modes within a 30–80-day period is given above the upper panel.

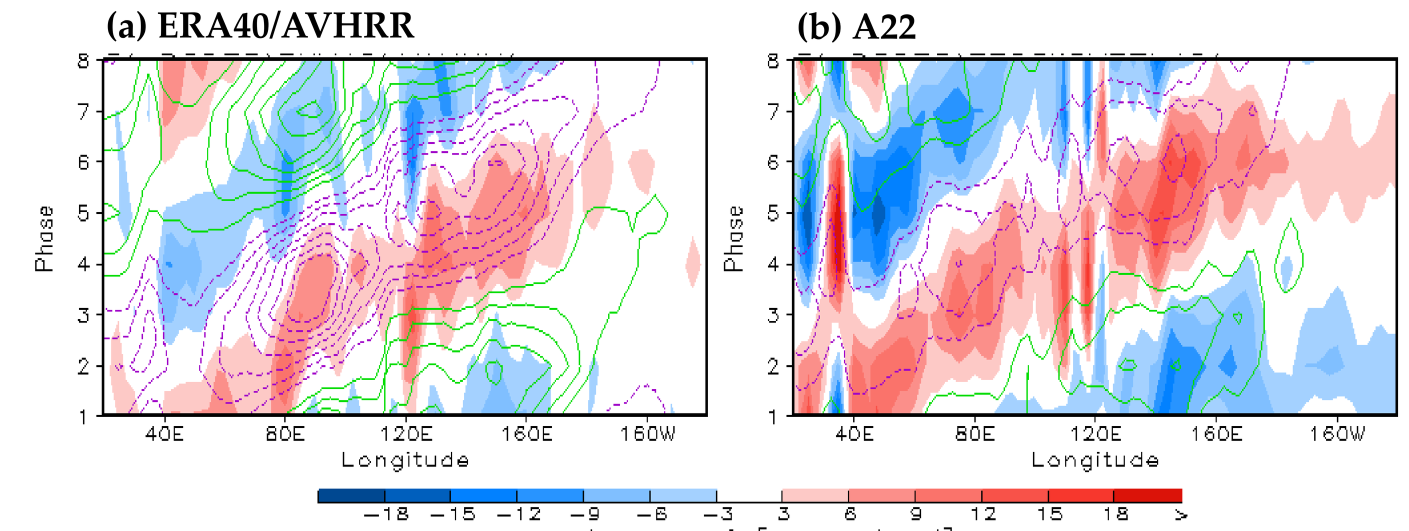

FIG. 5. Phase–longitude diagram of OLR [contour plotted every 3 W m^{-2}, positive (green) and negative (purple)] and 925-hPa moisture convergence (kg kg^{-1} s^{-1}, shaded). (a) ERA40/AVHRR, (b) A22. Phases are from MJO life cycle composite and values averaged between 10ºS and 10ºN.

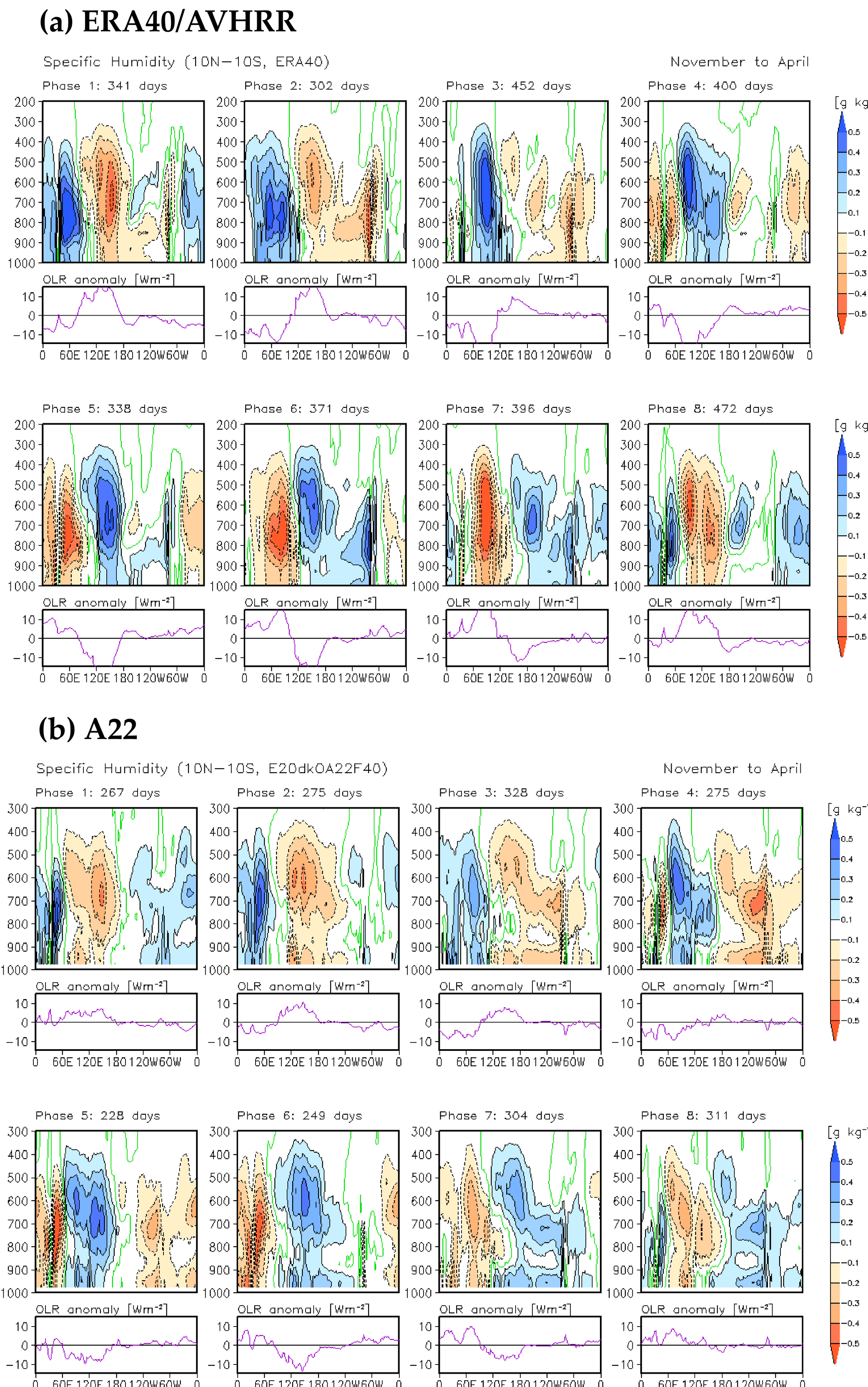

FIG. 6. Pressure–longitude diagram of OLR (W m^{-2}, lower panels) and specific humidity (kg kg^{-1} , upper) at each phase of MJO life-cycle. (a) ERA40/ AVHRR, and (b) A22.

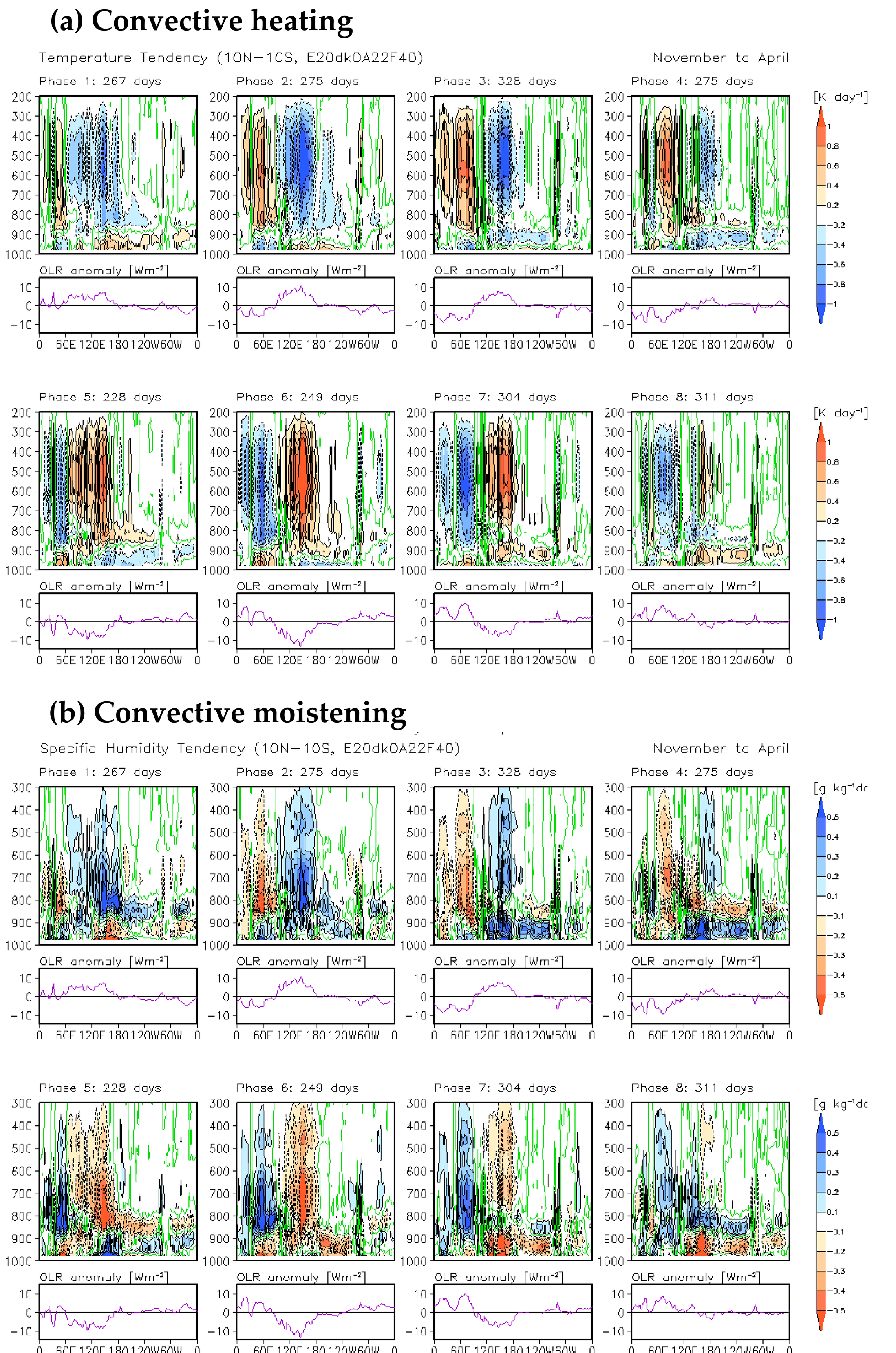

FIG. 7. Pressure–longitude diagram of OLR (W m^{-2}, lower panels) and (a) convective heating (K day^{-1} , upper) and (b) convective moistening (g kg^{-1} day^{-1}) at each phase of MJO life-cycle.

Process-oriented diagnostics

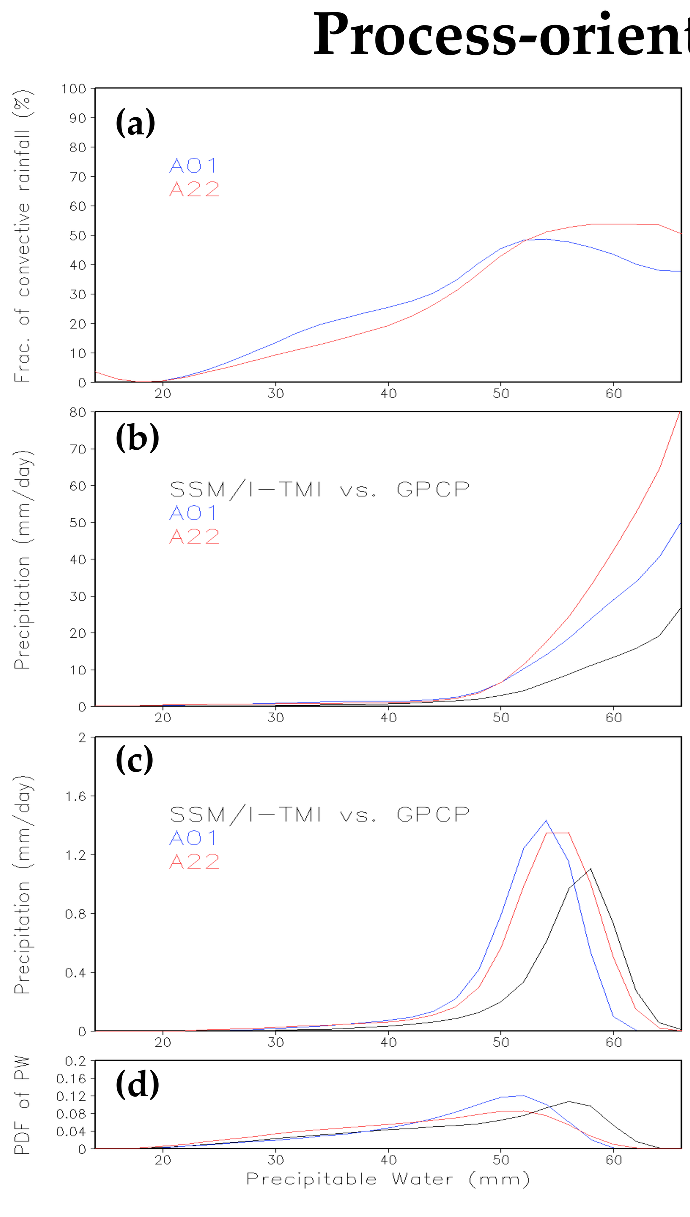

FIG. 8. Composites based on precipitable water. (a) fraction of convective rainfall, (b) precipitation, (c) pdf-weighted precipitation, and (d) pdf of precipitable water. Black: SSM/I-TMI and GPCP, Blue: AR5(A01), Red: A22

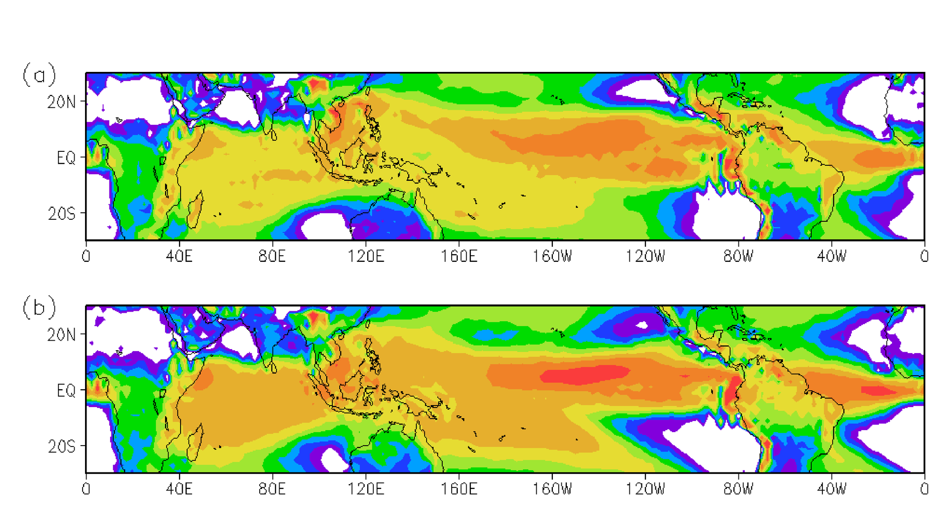

FIG. 9. November-April mean convective rainfal fraction (%)

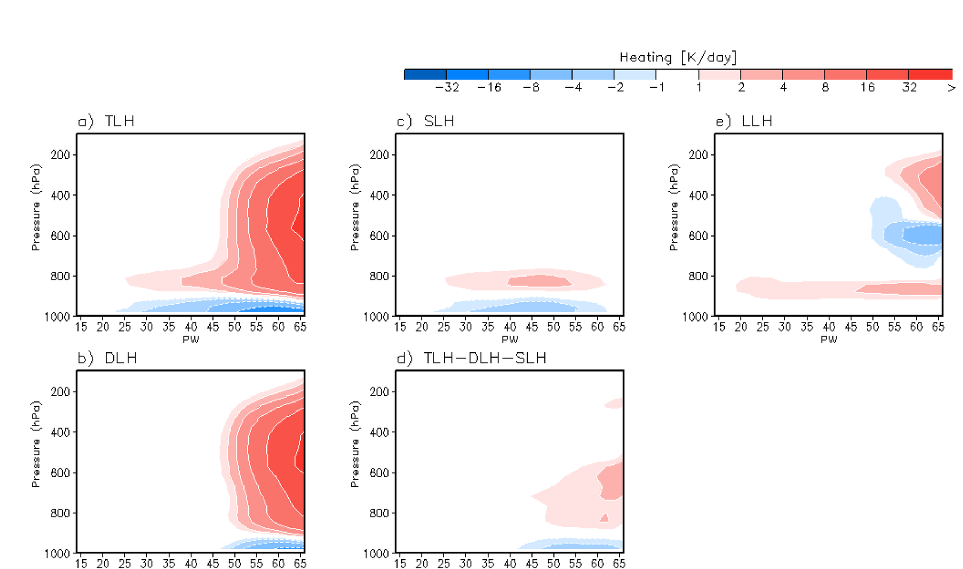

FIG. 10. Diabatic heating composite based on precipitable water (a) TLH (total convective), (b) DLH (deep convective), (c) SLH (shallow convection), (d) TLH-DLH-SLH (congestus), and (e) LLH (large-scale condensation). A22 result is used and the unit is K day^{-1}.

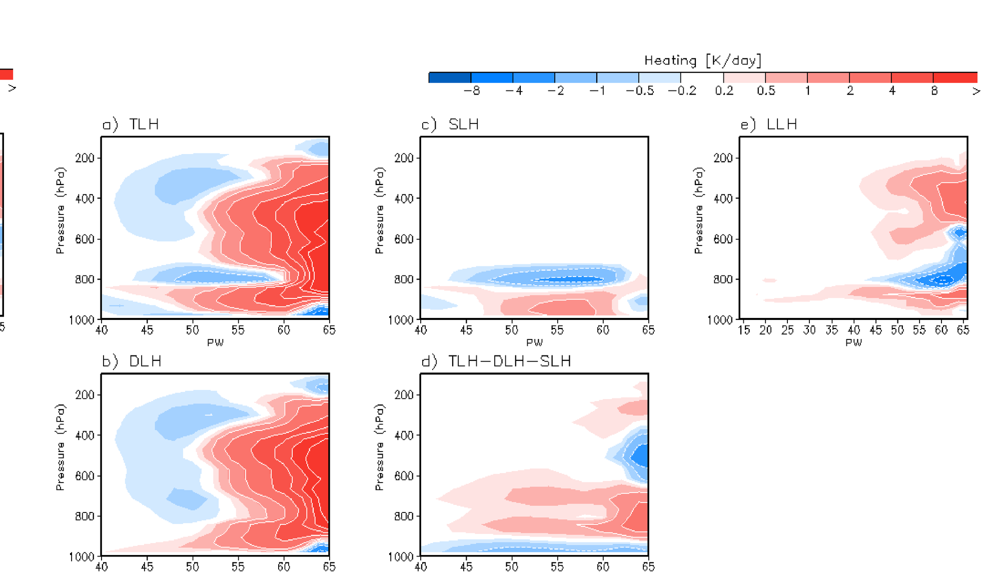

FIG. 11. Same as FIG. 10, except for difference between A22 and AR5 (A01).

CONTACT: Daehyun Kim
daehyunk@gmail.com; dkim@ldeo.columbia.edu